



## Research Article

# Turn Up the Lights, Leave them On and Shine them All Around—Numerical Simulations Point the Way to more Efficient Use of Far-UVC Lights for the Inactivation of Airborne Coronavirus

Kenneth Wood<sup>1\*</sup> , Andrew Wood<sup>2</sup>, Camilo Peñaloza<sup>1</sup> and Ewan Eadie<sup>3</sup> 

<sup>1</sup>SUPA, School of Physics & Astronomy, University of St Andrews, St Andrews, UK

<sup>2</sup>Fluid Gravity Engineering, St Andrews, UK

<sup>3</sup>NHS Tayside, Photobiology Unit, Ninewells Hospital and Medical School, Dundee, UK

Received 13 May 2021, accepted 15 September 2021, DOI: 10.1111/php.13523

## ABSTRACT

It has been demonstrated in laboratory environments that ultraviolet-C (UVC) light is effective at inactivating airborne viruses. However, due to multiple parameters, it cannot be assumed that the air inside a room will be efficiently disinfected by commercial germicidal ultraviolet (GUV) systems. This research utilizes numerical simulations of airflow, viral spread, inactivation by UVC and removal by mechanical ventilation in a typical classroom. The viral load in the classroom is compared for conventional upper-room GUV and the emerging “Far-UVC.” In our simulated environment, GUV is shown to be effective in both well and poorly ventilated rooms, with greatest benefit in the latter. At current exposure limits, 18 commercial Far-UVC systems were as effective at reducing viral load as a single upper-room GUV. Improvements in Far-UVC irradiation distribution and recently proposed increases to exposure limits would dramatically increase the efficacy of Far-UVC devices. Modifications to current Far-UVC devices, which would improve their real-world efficacy, could be implemented now without requiring legislative change. The prospect of increased safety limits coupled with our suggested technological modifications could usher in a new era of safe and rapid whole room air disinfection in occupied indoor spaces.

## HIGHLIGHTS

- For reducing virus concentrations, mechanical ventilation with the addition of an upper-room GUV device outperforms Far-UVC devices operating within current threshold limit values
- The proposed factor of twenty increase for Far-UVC threshold limit values will greatly increase the efficacy of Far-UVC devices
- Far-UVC devices will be most effective if they are on continuously have a wide illumination pattern and can operate at intensity levels above the current threshold limit values.

## INTRODUCTION

The germicidal properties of ultraviolet (UV) light have been known since the 1870s (1) with the mechanism of action believed to be that UV photons break bonds in DNA and RNA thereby destroying bacteria and inactivating viruses by preventing them from replicating (2). The most common form of germicidal ultraviolet (GUV) light used for disinfection is from low-pressure mercury vapor lamps. These lamps emit primarily at 254 nm, which is close to the peak of the UV germicidal response curve. Since the early twentieth century, such devices have been used in a variety of settings including water treatment, heating, ventilation and air-conditioning systems, disinfection of air and surfaces in hospitals, and for the prevention of the spread of airborne diseases such as measles and tuberculosis (1).

The UV light from mercury lamps can cause skin and eye damage in the form of erythema and photokeratitis. Therefore, safety considerations require that such lamps must be operated in unoccupied spaces or designed so that their light is confined to a region above head height to prevent direct exposure, with such devices known as upper-room GUV.

In recent years, a new GUV technology has emerged employing Krypton Chloride (KrCl\*) excimer lamps that emit primarily at 222 nm, commonly referred to as Far-UVC. These shorter UV wavelengths have similar germicidal properties to the conventional mercury vapor lamps (3,4), but theoretical and experimental studies indicate such devices may be safe to use in occupied spaces because the stratum corneum (the outermost layer of the skin) and the tear layer of the eye provide natural protective barriers (3–10). Provided the harmful emissions from wavelengths beyond 230 nm can be reduced through filtering (11,12), this raises the prospect that appropriately filtered Far-UVC devices could be used continually in occupied spaces to prevent the airborne spread of bacteria and viruses, including SARS-CoV-2, the virus responsible for the COVID-19 pandemic. In addition to reducing airborne pathogens, Far-UVC devices may also be used alongside manual cleaning for surface disinfection (13).

However, there is little real-world evidence available for commercially available far-UVC devices. Previous computer modeling has investigated the efficacy of upper-room GUV in hospital

\*Corresponding author email: kw25@st-andrews.ac.uk (Kenneth Wood)  
© 2021 American Society for Photobiology

wards, concluding they are most efficient in settings with poor ventilation (14,15). They can routinely achieve the equivalent of twenty-four air changes per hour (ACH) and even up to one hundred ACH (16). ACH is a theoretical construct where in a room, with good air mixing, one air change will remove  $(1 - 1/e) \approx 63\%$  of the pathogens. The second air change removes 63% of the remaining pathogens and so on, so that after  $N$  air changes, the remaining fraction of pathogens is  $e^{-N}$ . The recommended ACH varies according to a room's use, but typically well-ventilated rooms are those with 6ACH to 12ACH. Poor ventilation is represented by  $<2$ ACH.

A recent computer simulation of Far-UVC inactivation of coronavirus (17) investigated a two-dimensional single occupancy hospital room of 3 m by 3 m with mechanical ventilation from a single inlet with inflow speeds to mimic 1ACH and 8ACH. An isotropic source of 222 nm continually irradiated the room, and the light's power was set so that it delivered a fluence rate at head height close to the current threshold limit value (TLV). For 222 nm, the current TLV is  $23 \text{ mJ cm}^{-2}$  in an eight-hour period (18), which is equivalent to receiving a continuous fluence rate of  $0.8 \text{ } \mu\text{W cm}^{-2}$  for 8 h. As with the upper-room simulations, the largest reduction in viral loads was observed for low ACH.

We wished to expand upon previous studies by modeling in three dimensions and using measured values as input parameters. Using a combination of computational fluid dynamics, particle dissemination and three-dimensional light distributions from commercially available GUV devices, we construct computer simulations of the inactivation of airborne viruses in a realistic classroom environment. We present results for the time-dependent decrease of the viral load within the classroom by ventilation and UVC inactivation, comparing upper-room and Far-UVC GUV devices. We study the efficacy of the GUV devices for different ventilation rates, and the number, location and irradiance distribution of Far-UVC devices. We construct simulations where the Far-UVC devices operate within the current safety exposure limits defined by the TLV, but also investigate virus inactivation times for higher TLVs that have been proposed in light of the recent research indicating the safety of appropriately filtered Far-UVC lights (19).

## MATERIALS AND METHODS

*Numerical simulations of virus inactivation.* Our simulations are based on a classroom in the School of Physics and Astronomy at the University of St Andrews. This room was chosen because it has dimensions typical of a medium-sized teaching room that accommodates approximately thirty students. The room has mechanical ventilation with four air inlets and outlets through three open windows. The height of the room is also suitable for upper-room GUV.

Computational fluid dynamics simulations should be validated against real-world experimental data. This has been done for upper-room GUV devices in a hospital ward with similar dimensions to our simulated classroom and also in a bioaerosol chamber (14,15). We are planning similar live-testing of Far-UVC devices in a bioaerosol chamber alongside numerical simulations of airflow, virus spread and UVC inactivation. Results of the live-testing and validation of numerical simulations will be reported in future papers.

Steady-state airflow is computed and particles are treated as passive tracers, similar to published studies (15). The viral reduction due to inactivation by UVC light is computed by adopting decay constants from aerosolizing chamber experiments (3). Details of the fluid dynamics, particle dissemination, UVC fluence rates and virus inactivation are given below.



**Figure 1.** Room 230 in Physics & Astronomy at the University of St Andrews. Three of the four air inlets can be seen on the right near the ceiling opposite the three windows on the left side of this classroom.

*Room geometry and ventilation.* Room 230 in the School of Physics and Astronomy at the University of St Andrews, shown in Fig. 1, has dimensions 12 m by 5.9 m by 3 m. Mechanical ventilation is provided by four air inlets that are each 20 cm by 20 cm. The inlets are all positioned on one side of the room with three tilt windows on the opposite side. Three of the air inlets are mounted on the wall at a height of 2.5 m above ground and the fourth is in the ceiling. We measured the air inflow speed with an anemometer to be around  $2.5 \text{ ms}^{-1}$  which gives a ventilation rate of 6.8ACH.

The purpose of our study is to compare the efficacy of GUV devices, so we do not consider the fine details of the inlet velocity profiles, and for the simulations described below, we assume the inlets are all on the walls and the open windows are represented by outflow boundary conditions through gaps that are 131 cm by 10 cm. In addition, for this first study we assume the room is empty, so our simulations are not a replica, but rather they are inspired by Room 230. The results will of course change if furniture and other heat sources (radiators, people, etc) are included. Studies of upper-room devices indicate these additional complexities have a lesser effect on the GUV efficacy compared with the ventilation airflow and light distributions (15).

*Steady-state airflow.* To calculate the flow fields, a similar approach to published studies is taken (15). The open-source computational fluid dynamics (CFD) software package, OpenFOAM (20), is used to calculate steady-state, incompressible solutions of the Reynolds-averaged Navier-Stokes equations:

$$\nabla \cdot \mathbf{u} = 0 \quad (1)$$

$$\mathbf{u} \cdot \nabla \mathbf{u} = -\nabla p + \nu \nabla^2 \mathbf{u} - \nabla \cdot \overline{\mathbf{u}'\mathbf{u}'} \quad (2)$$

where  $\mathbf{u}$  is the velocity field,  $p$  the kinematic pressure,  $\nu$  the kinematic viscosity and  $\overline{\mathbf{u}'\mathbf{u}'}$  the kinematic Reynolds stress tensor.

The room is modeled as a simple cuboid domain of dimensions 12 m by 5.9 m by 3 m. The four inlets are modeled as 20 cm by 20-cm square patches, positioned on one of the 12-m walls so that their top edges are 30 cm below the ceiling. The three outlet windows are modeled as 131 cm by 10 cm rectangular patches, positioned 1 m above the floor on the opposite 12-m wall.

Inflow is modeled as a constant, uniform velocity profile across each inlet, normal to the wall. The same inflow velocity is applied at each inlet, with values of  $2.5 \text{ m s}^{-1}$  and  $0.5 \text{ m s}^{-1}$ , in two CFD simulations, giving ventilation rates of 6.8ACH and 1.4ACH, respectively. A no-slip boundary condition is applied to the velocity at the walls, floor and ceiling. A fixed value pressure boundary condition is applied at the outlets.

Turbulence is modeled with the standard k- $\epsilon$  model. Fixed values of  $0.016 \text{ m}^2 \text{ s}^{-1}$  and  $0.014 \text{ m}^2 \text{ s}^{-3}$  are applied at the inlets to  $k$  and  $\epsilon$ ,

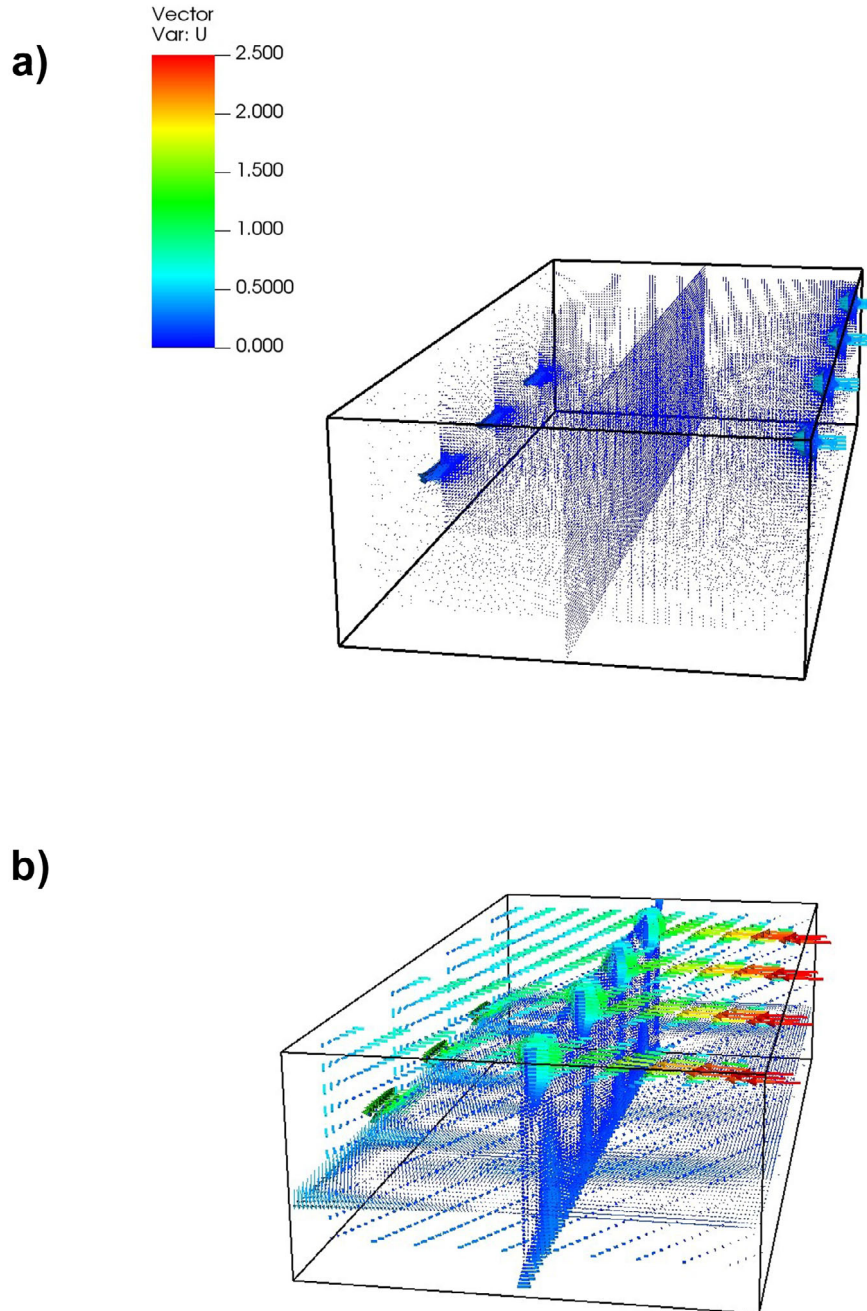


**Figure 2.** Steady-state velocity fields displayed in units of  $\text{m s}^{-1}$  from OpenFOAM simulations with 1.4ACH and 6.8ACH. The images show representative slices of the velocity fields in vertical and horizontal planes. The four air inlets are on the upper right hand sides and the three windows on the lower left sides.

respectively. These are arbitrary values since we have no data at present on the turbulent properties at the inflow. A zero gradient boundary condition is applied to  $k$  and  $\epsilon$  at the walls, floor and ceiling.

A uniform mesh is used with a cell size of 5cm, which is just small enough to resolve the inlets and outlets. The resulting steady-state velocity fields for simulations with 1.4ACH and 6.8ACH are shown in Fig. 2. We have deferred mesh resolution and parameter sensitivity studies for future work.

*Particle dissemination.* Virus particles are assumed to be held in suspension inside aerosolized drops of liquid that have been exhaled by an infected individual. Following (15), the dissemination of such drops is calculated by integrating the equations of motion for a particle moving through a gas, subject to drag and gravity:

$$\frac{d\mathbf{x}_p}{dt} = \mathbf{u}_p \quad (3)$$

$$m_p \frac{d\mathbf{u}_p}{dt} = \frac{C_d \pi r_p^2}{2} \|\mathbf{u}_p - \mathbf{u}(\mathbf{x}_p)\| (\mathbf{u}_p - \mathbf{u}(\mathbf{x}_p)) + m_p \mathbf{g} \quad (4)$$

$$C_d = 0.42 + \frac{24}{Re} + \frac{4.4}{\sqrt{Re}} \quad (5)$$

where  $r_p$  and  $m_p$  are the radius and mass of the drop,  $\mathbf{x}_p$  and  $\mathbf{u}_p$  the position and velocity of the drop,  $C_d$  the drag coefficient and  $Re$  the particle Reynolds number.

In the limit of zero radius, these equations reduce to

$$\frac{d\mathbf{x}_p}{dt} = \mathbf{u}_p = \mathbf{u}(\mathbf{x}_p) \quad (6)$$

The fluid velocity,  $\mathbf{u}(\mathbf{x}_p)$ , is calculated by linear interpolation of the values at adjacent grid points calculated by OpenFOAM. Diffusion due to turbulence or Brownian motion has been neglected in these equations.

Since we assume the overall loading density of aerosolized drops is too small to affect the fluid flow, Eqs. 3–6 can be solved separately from the CFD calculations and this is done as a post-processing step using Fluid Gravity Engineering's dissemination code, EFFECTS. Therefore, for any given flow field, it is only necessary to perform the CFD calculation once. Since the post-processing calculations of particle trajectories, radiation field and virus inactivation are computationally inexpensive in comparison with the CFD, many different particle distributions and lighting configurations can be studied for a given flow field allowing a large region of the parameter space to be explored efficiently.

This research considers the limiting case of zero-radius particles, so that equation 6 applies and the particles behave as passive tracers following the fluid flow. The trajectories of 7080 particles are calculated. Their initial positions are distributed uniformly in a grid in the horizontal plane 0.5 m above the ground with a separation of 10 cm between adjacent particles. The data set produced allows the particle distribution to be varied without repeating the calculation of the trajectories. For instance, the initial spatial distribution can be varied by selecting a suitable subset of particles from the data set or by applying appropriate weights to different particles. Since we are considering steady-state fluid flow, continuous release of particles can be modeled using time-shifted copies of existing trajectories in the data set. Our simulations are likely to be best outcomes as including furniture and other heat sources could lead to more complex airflow patterns with possible stagnation regions and furniture can create shadowed areas where Far-UVC downlights cannot reach. We will consider such scenarios in a future project.

**UVC fluence rate.** The three-dimensional fluence rates arising from the GUV devices are computed throughout the room using a Monte Carlo radiation transfer (MCRT) code originally developed for astronomy research (21), but subsequently adapted to compute 3D light distributions and fluence rates in biological tissue (22), and now rooms for the present study.

The MCRT code can simulate the emission, scattering and absorption of light within a 3D medium with optical properties discretized onto a 3D linear Cartesian grid. For the simulations in this paper, the number of grid cells in the  $x$ ,  $y$  and  $z$  dimensions is 100, 200 and 50 which then allows the fluence rate to be determined in the one million cubical cells that are each 6cm on a side. Scattering and absorption are not considered within the room because the attenuation coefficient for Rayleigh scattering and absorption in air is of order  $10^{-5} \text{ m}^{-1}$  at 222 nm (17). The walls and ceiling are treated as diffusively reflecting surfaces and assigned a reflection coefficient of 10% which is typical of painted and tiled surfaces at UVC wavelengths (23).

The Far-UVC devices are assumed to be mounted in the ceiling and emit photons into the downward hemisphere. Although the emission of UV photons from a KrCl\* bulb is isotropic, the requirement of filters to suppress the harmful longer UVC wavelengths and lamp housing leads to a narrow illumination pattern from all current commercially available filtered Far-UVC devices. In our simulations, we compare a typical illumination pattern from a commercially available Far-UVC device with a pattern that is isotropic in the downward direction (i.e., equal number of photons are emitted into equal solid angles). The fluence rates for these two azimuthally symmetric illumination patterns are displayed in Fig. 3 which shows the pattern of the commercial device is considerably narrower than the isotropic pattern. The fluence rates for the two different illumination patterns and different numbers of Far-UVC lights are depicted in the 3D images in Fig. 4.

All GUV devices must operate within the regulatory framework defined by the TLV, which at 222 nm corresponds to a continual fluence rate of  $0.8 \mu\text{W cm}^{-2}$  in an eight-hour period. In order to simulate this, the power output of the Far-UVC lights is scaled so that they do not exceed this fluence rate anywhere in a horizontal plane at a height of 2 m above the ground. This is an extremely conservative interpretation of the TLV and is equivalent to assuming a 2-m tall person stands in the same location for 8 h. In most of our simulations, we

assume the Far-UVC devices operate continually. This is different from current commercial practices, but as we will discuss below, straightforward modifications can allow Far-UVC devices to operate continually.

For the upper-room device, we assume it is mounted 30 cm off the center of the wall opposite the air inlets at a height of 2.1 m. Photons are emitted from a plane 40 cm by 20 cm with an isotropic distribution extending to  $5^\circ$  in latitude and  $\pm 45^\circ$  in longitude. The distribution is tilted so that no photons are emitted below the horizontal. The resulting illumination pattern is shown in Fig. 3 which is similar to that studied in previous research (23). The narrow latitudinal opening angle means that no photons will directly hit the ceiling, and the UV power output is set so that the fluence rate in the lower room does not exceed the 254 nm TLV which corresponds to  $0.2 \mu\text{W cm}^{-2}$ . The fluence rate due to the upper-room device peaks at around  $20 \mu\text{W cm}^{-2}$  close to the device and is  $< 0.5 \mu\text{W cm}^{-2}$  at the opposite wall. The fluence rates in the upper room are significantly higher than the current TLV for Far-UVC devices, resulting in very rapid inactivation of virus particles that pass through the light path of the upper-room device.

**UVC inactivation.** As particles move within the flow field in the room, they are exposed to a spatially varying fluence rate. A general approach is to tally the cumulative UV dose that each particle receives in a specified time period (14). We also compute the virus inactivation as the particles move, in a similar manner to that of previously published Far-UVC simulations (17).

We assume viruses within the particles are inactivated according to an exponential decay,

$$N(t) = N_0 \exp \left[ -k_V \int_0^t \psi(x(t'), y(t'), z(t')) dt' \right], \quad (7)$$

where  $N_0$  and  $N(t)$  are the number of viable viruses in the particle at the start and after a time  $t$ ,  $\psi(x, y, z)$  is the 3D fluence rate ( $\text{mJ cm}^{-2} \text{ s}^{-1}$ ), and for both Far-UVC and upper-room simulations, we adopt the decay constant for HCoV-OC43  $k_V = 5.9 \text{ cm}^2 \text{ mJ}^{-1}$  as measured in aerosolizing chamber experiments (3).

## RESULTS

Our numerical simulations investigated two ventilation rates, one upper-room device, multiple numbers of Far-UVC devices with different illumination patterns, and three different TLVs. The results of these simulations are presented in Figs. 5 through 8 and described below.

### Number and location of far-UVC sources

To determine the effectiveness of UVC devices, we make comparisons with the removal of particles by ventilation. For the one-time release of particles, Fig. 5 shows that after one hour, the mechanical ventilation in our simulations has reduced the particle concentration to 37% of its initial concentration for 1.4ACH and 2% for 6.8ACH. The addition of an upper-room GUV device further reduces the concentrations to 5% for 1.4ACH and 0.2% for 6.8ACH. This is as expected where upper-room GUV devices are most efficient in rooms with poor ventilation (14,15).

The number of Far-UVC devices has a significant influence on the viral load. When operating at the current TLV, a single currently available commercial far-UVC device has only a small effect: For 1.4ACH, the particle concentration after one hour is 34% (compared to 37% with ventilation only), and for 6.8ACH, the concentration is 1.7% (compared to 2% with ventilation only).

Combined with mechanical ventilation, four such units in a line evenly spaced along the length of the room would reduce

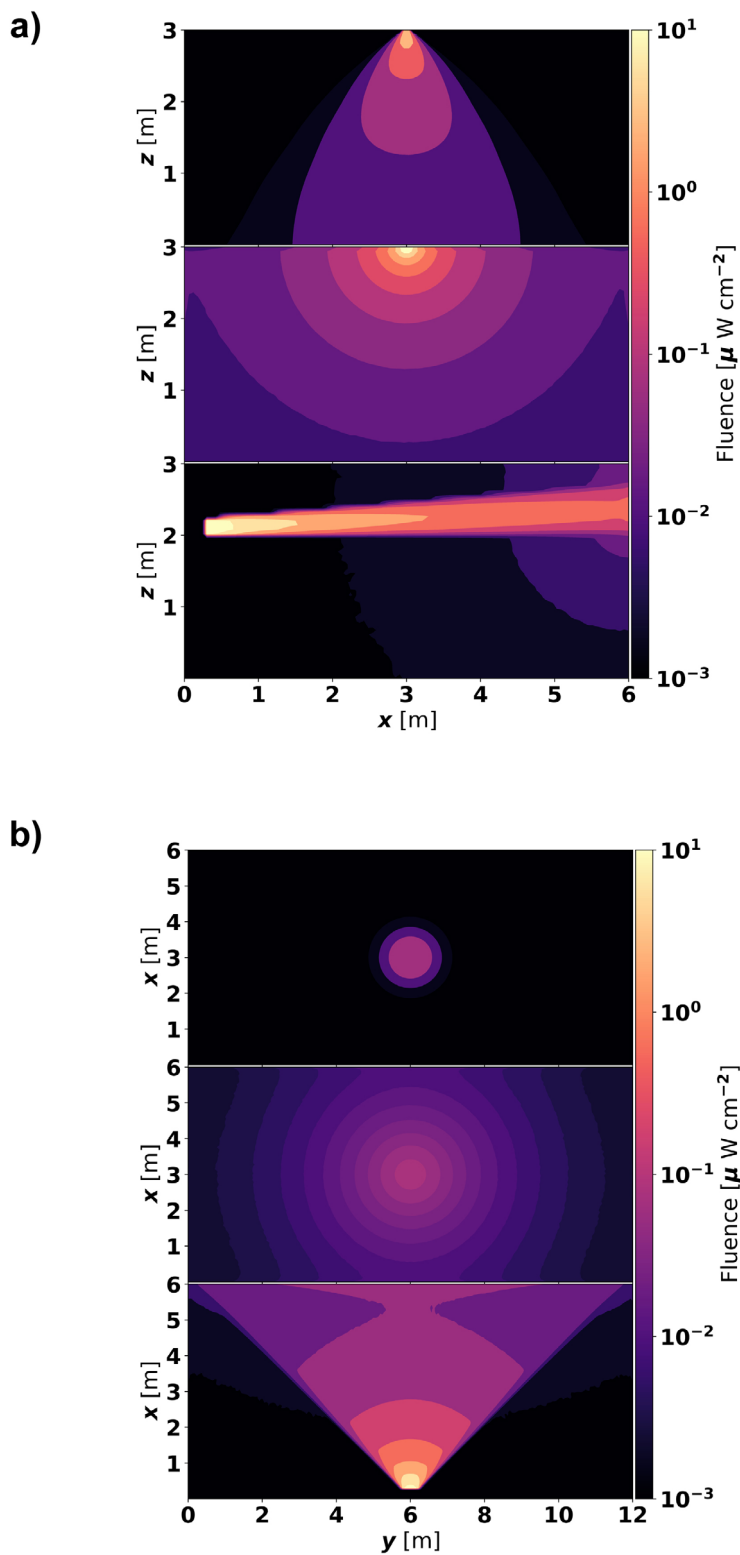
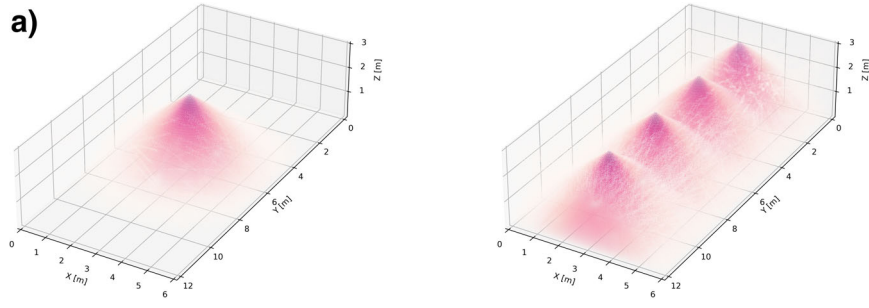
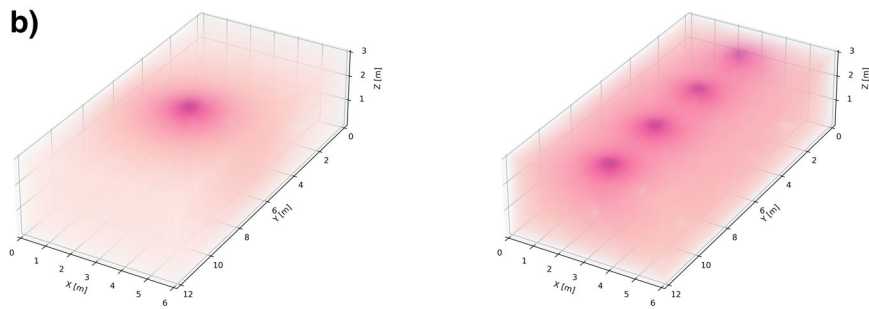
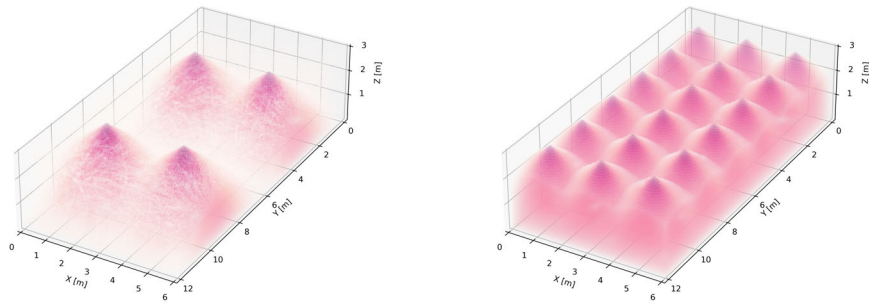


**Figure 3.** A one pixel-wide slice in the  $x-z$  (left) and  $x-y$  (right) planes showing the fluence rate patterns of a typical commercial Far-UVC device, an isotropic pattern, and a simulated upper-room device. The  $x-y$  fluence rate map is taken at a height of 2.2 m. The Far-UVC devices are shown with a scaling to provide a fluence rate appropriate for the current TLV at a height of 2 m. Notice that the upper-room device provides a much higher fluence rate than the Far-UVC devices in the area above head height, leading to rapid virus inactivation in this region. Low-intensity light from the upper-room device that is scattered from the walls and ceiling can be seen in the lower room regions.



**Fluence of Commercial Lamps**



**Fluence of Isotropic Lamps**

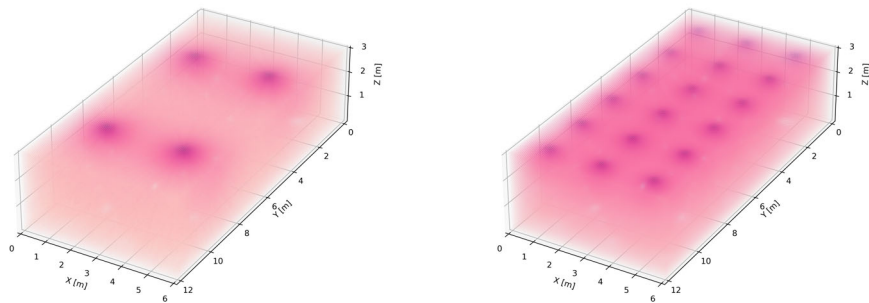


**Figure 4.** Three-dimensional representation of the fluence rates within the room for different Far-UVC lighting scenarios. Left four panels show fluence rates arising from the illumination pattern of typical commercial Far-UVC devices, right four panels for isotropic lights

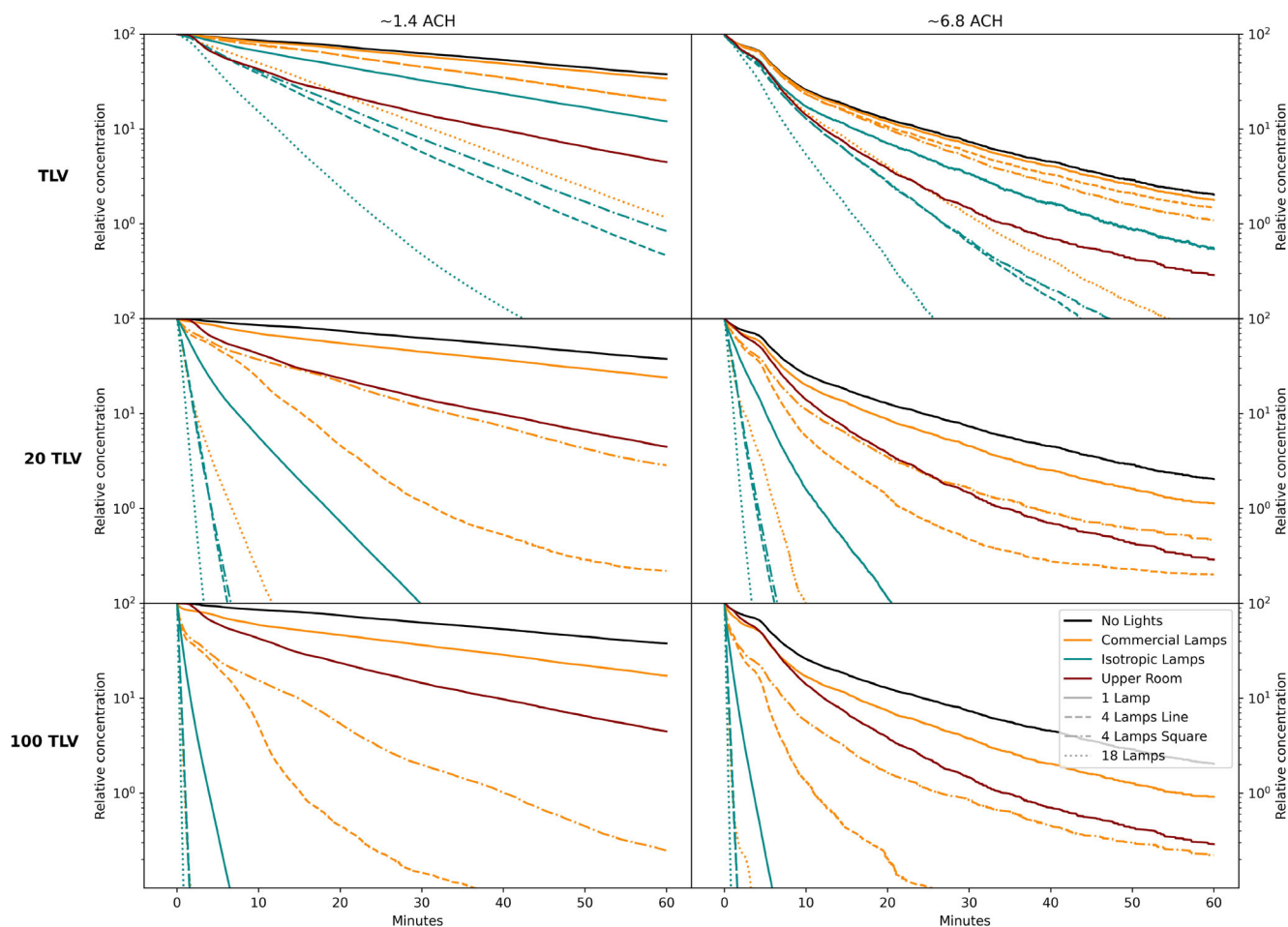


**Figure 5.** Relative concentrations as a function of time after a one-time release of particles within the room. Left panels are for simulations with 1.4ACH and right panels for 6.8ACH. The uppermost panels assume the Far-UVC lights operate continuously at the current TLV by delivering a maximum fluence rate of  $0.8 \mu\text{W cm}^{-2}$  at a height of 2 m. The middle and bottom panels increase these TLV fluence rates by a factor of twenty and one hundred, respectively. The different linestyles are displayed in the caption and explained in the text.

the viral concentration to 19% for 1.4ACH (37% ventilation only). There is a dramatic increase in the viral reduction if eighteen of the commercial units are used, as is currently recommended by manufacturers for a classroom of this size. In this scenario, the concentration is reduced to 1.2% after one hour (37% for ventilation only), which is a higher reduction than upper-room GUV (5%).

The effect is less marked in a room with better ventilation. For the scenarios described above for the 6.8ACH simulations, after one hour the viral concentration is reduced to 1.7% for one lamp, 1.4% for four lamps and 0.07% for eighteen lamps (compared to 2% with ventilation only and 1% for upper-room GUV).

In a one-time release scenario, 6.8ACH initially reduces the viral load faster, but with eighteen far-UVC devices, the viral load is overall lower after sixty minutes in the room with 1.4ACH (1% relative concentration for 1.4ACH vs 2% relative concentration for 6.8ACH). In an arguably more realistic scenario however, with continual viral release (Fig. 6), the improved ventilation of 6.8ACH outperforms any added benefit of the Far-UVC devices in the room with 1.4ACH. Both the recommended

18 commercial Far-UVC units and a single upper-room GUV unit provide an approximately equal reduction in viral load in the continual release scenario.

In a scenario with limited Far-UVC lamp coverage, changing the location of the lights within the room also has an influence on the results. Arranging the four lights in a row provides very similar whole room viral inactivation to four lights in a square pattern. While true in an average whole room scenario, the result is very dependent on the source of virus particles and the details of the ventilation airflow pattern (See Section “Location dependence”). Optimizing the Far-UVC light distribution in a room should not only consider the illumination pattern but also the specifics of the ventilation.

#### Far-UVC illumination pattern

Far-UVC devices with an isotropic illumination pattern (i.e., wider distribution of UV light) as shown in Figs. 3 and 4 allow photons to reach more of the room resulting in greater inactivation. In a one-time release scenario, at current TLV in a room with 1.4ACH, four far-UVC lamps with an isotropic

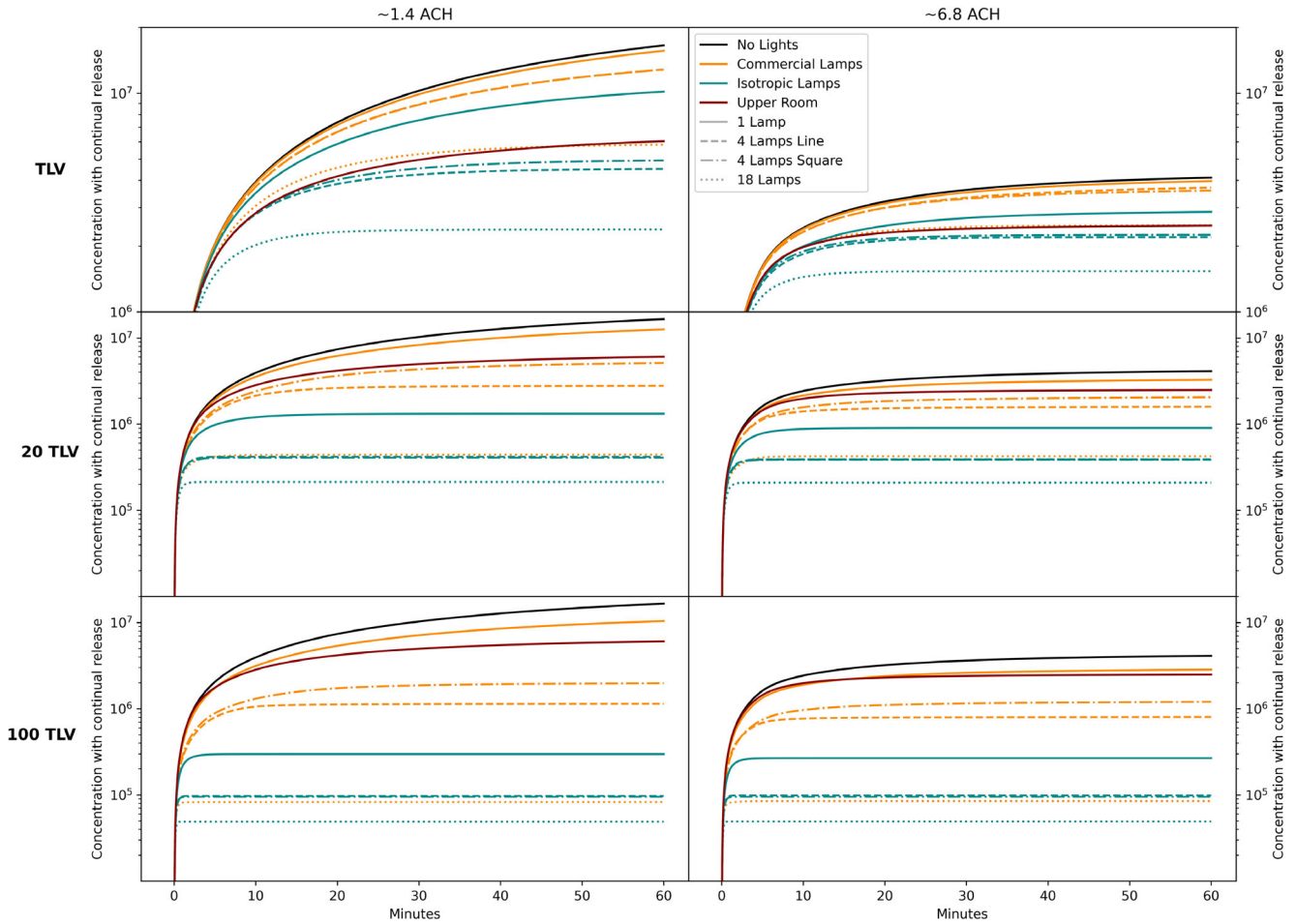


**Figure 6.** As for Fig. 5, but for ‘continuous release’ where 7080 particles are released from a height of 0.5 m (as described in the Section ‘Particle dissemination’) every second of the simulation

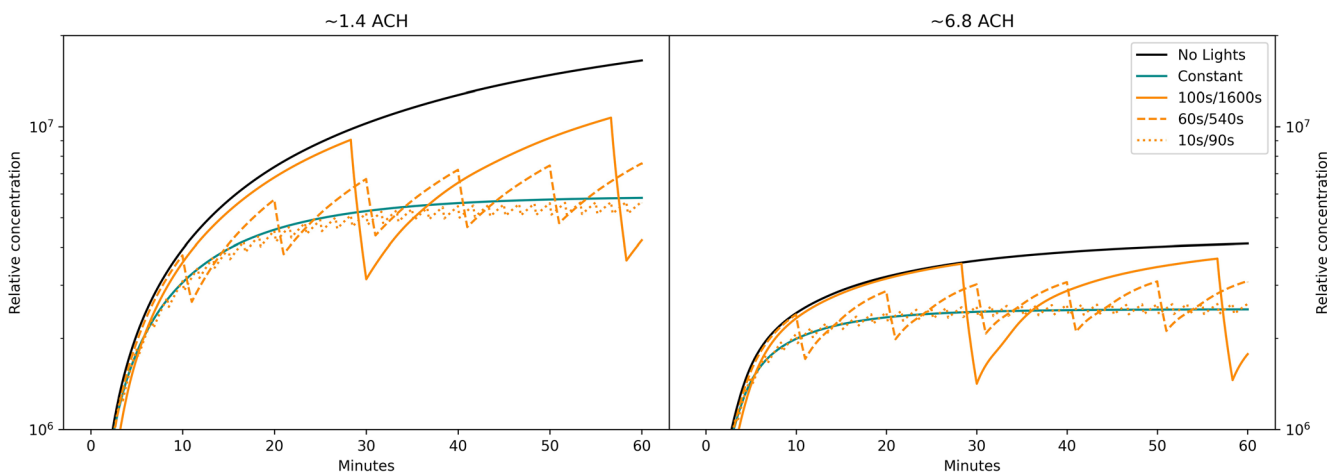


**Figure 7.** As for Fig. 6, but now comparing ventilation with eighteen commercial devices operating either in continuous mode or on duty cycles with on/off times as indicated.

distribution would outperform eighteen of the commercially available systems at sixty minutes: concentrations being 0.5% for four isotropic compared with 1.2% for

eighteen commercial lights. Combined with ventilation, eighteen isotropic lights would achieve a 99.9% reduction in particle concentration in 42 min (1.4ACH) and 25 min (6.8ACH).



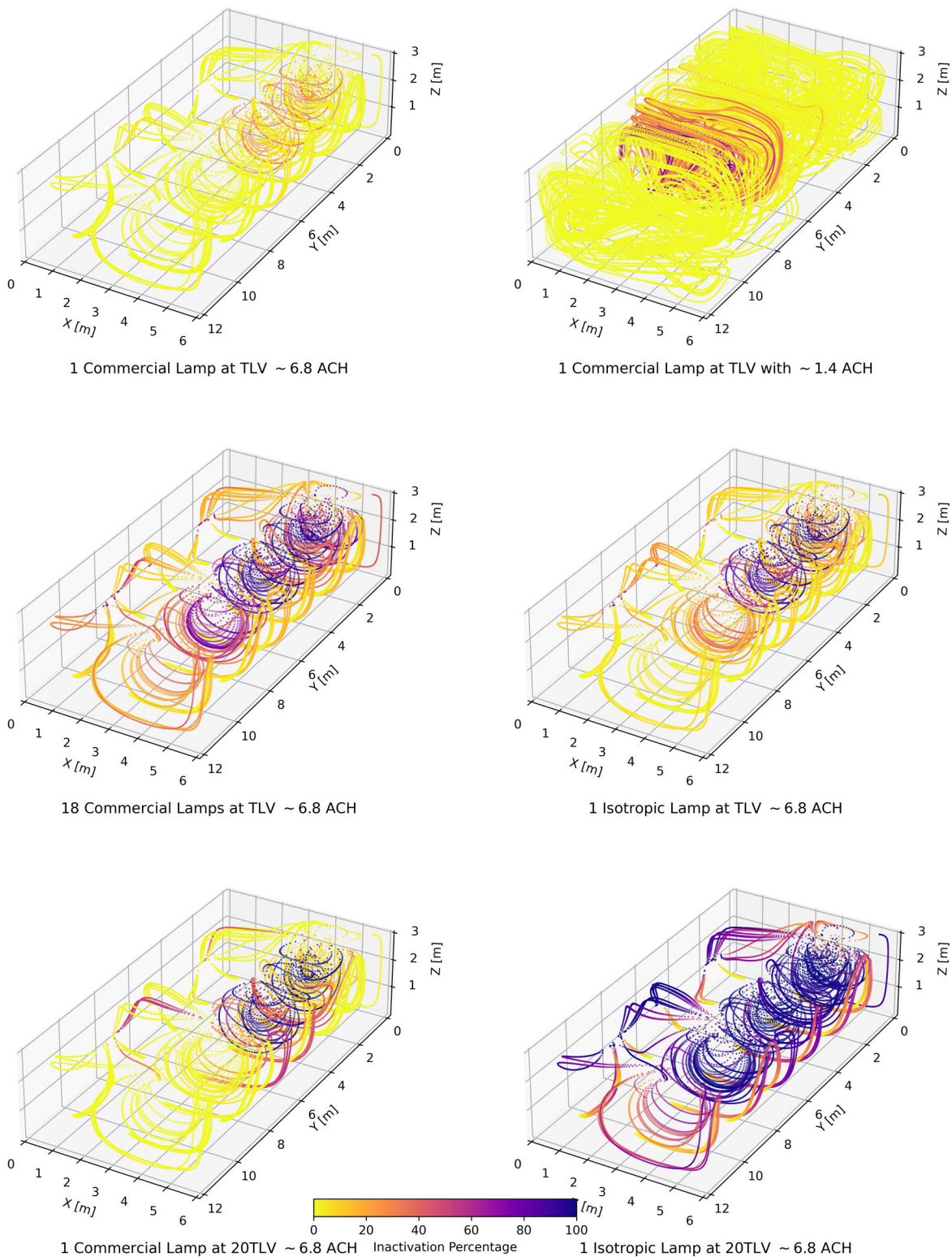


**Figure 8.** Example of particle trajectories for different irradiation and intensity patterns for Far-UVC devices. Unless otherwise stated, the airflow is for the simulation with 6.8ACH. In each of the figures, the air inlets are on the right and the particle trajectories can be seen exiting the three open windows on the left. The trajectories display the inactivation as a function of position where a particle is emitted either for an hour of elapsed time that the simulation represents or until it exits the simulation via a window. Note the bottom right figure that shows the rapid inactivation achievable for a single isotropic light that delivers twenty times the current TLV at a height of 2 m

### Threshold limit value

The single parameter that has the greatest influence on the ability of Far-UVC devices to decrease the viral load in a room is the TLV. The middle panels in Fig. 5 show that in a one-time release scenario, in a room with 1.4ACH and a TLV at twenty times its current value, one isotropic far-UVC source would achieve 99.9% reduction in 29 min, far superior to eighteen commercial sources operating at the current TLV. Increasing the TLV by a factor of one hundred would result in the same reduction in viral load in just 6 min. Additional far-UVC sources also improve the 99.9% inactivation time: Eighteen isotropic far-UVC sources achieve this in 3 min at twenty times the current TLV and 45 s at one hundred times the current TLV.

In a continual release scenario, increasing the TLV results in far-UVC being the predominant reduction factor rather than ventilation or the addition of an upper-room GUV device. At twenty times the current TLV with four isotropic far-UVC sources, the viral load is approximately the same for a room with 1.4ACH or 6.8ACH. At twenty times the current TLV, as recently proposed by the ACGIH (19), four of the commercially available far-UVC systems in a room with 1.4ACH would be effectively the same as having a room with 6.8ACH.

### Duty cycles

Currently available Far-UVC devices that use KrCl\* bulbs employ duty cycles so that their time-averaged output stays within the TLV. Typically, the on/off time of the devices depends on their location within a room and is set so that the time-averaged dose received at a height of 1.7 m does not exceed  $23 \text{ mJ cm}^{-2}$  in 8 h. For the classroom simulations we have considered, this would mean that some current commercial devices would operate on a duty cycle being on for under a minute and then off for up to 10 min or longer. In such a scenario with a 10% duty cycle, when the Far-UVC device is on it would deliver a fluence rate equivalent to ten times the current TLV. But when the device is off virus particles will continue to spread throughout the room, subject only to removal through ventilation.

Some Far-UVC devices that operate on duty cycles will provide short bursts of air decontamination and may be useful in short-time occupancy environments such as lavatories and elevators, but in their current mode of operation, such devices would not be able to provide continual disinfection of air in rooms where people congregate for long periods of time. In a classroom environment for example, such devices could provide air disinfection between classes, but would be limited in their ability to provide a safe environment during a typical hour-long meeting. Using neutral density filters to reduce the output power will allow Far-UVC devices to operate continually within the TLV to disinfect air in occupied rooms.

Figure 7 shows simulations comparing ventilation, continual operation of eighteen commercial lights and lights operating on three different duty cycles with on/off times of 100s/1600s, 60s/540s and 10s/90s. As expected, the viral load increases during long off times and the duty cycles with shorter off times are preferred.

### Location dependence

The previous sections consider the “whole room” situation with an even release of particles at all locations in the room. This

provides a steady-state situation and allows for the effects of the different variables to be investigated. In reality, any virus release is likely to be more localized and the effect of the Far-UVC sources on those particles will depend upon the release point of the particles as well as the air flow in the room.

Figure 8 shows a selection of paths of particles during a one-hour period, as they move from their point of emission. Paths are color coded according to the extent of viral inactivation that occurs as the particles move within the 3D light distributions. Most of the panels are for simulations with 6.8ACH, and particle trajectories can be seen circulating in the room and eventually leaving through the open windows. For 1.4ACH simulations, the particles can get caught up in circulation patterns and spend much more time in the room; hence, the density of trajectories is higher. The figure shows different scenarios ranging from a single commercial light in a poorly ventilated room to isotropic lights operating at an increased TLV in a well-ventilated room. Similar figures showing accumulated UV dose from upper-room devices have been presented in other works (15).

A single commercial device operating at the current TLV does not provide much air disinfection in a room with 6.8ACH (Fig. 8, top left panel). It does better in a poorly ventilated room (top right panel), but only for particles that are toward the center of the room and can pass through its irradiation distribution.

Increasing the number of commercial lights (middle left panel) gives better room coverage and more virus inactivation. The whole room inactivation figures show that a single isotropic light provides almost the same inactivation as eighteen commercial lamps, and this is demonstrated in the inactivation trajectories (middle right panel).

When discussing the whole room inactivation plots, we stated that the single parameter that has the greatest effect is the TLV. This is clearly shown by the inactivation trajectories of the bottom panels where a single commercial light (bottom left panel) and single isotropic light (bottom right) are shown for a simulation of 6.8ACH and TLV increased by a factor of twenty.

The inactivation trajectories show that for some situations, particles that leave by the windows have not attained much of a UV dose and hence little virus inactivation. Also, although providing full room disinfection, rapid close range infection will not necessarily be stopped by Far-UVC. This is not surprising and such a situation where airflow impacted virus transmission has been described where diners in a restaurant who were sitting in the airflow of an infected person developed COVID-19 (24). Careful consideration must be given to ventilation and seating patterns within indoor venues.

### UV susceptibility

The inactivation of viruses by GUV light has been modeled using the single parameter  $k_V$  in equation 7 which takes larger values for viruses that are more susceptible to UVC light. In the simulations presented so far, we have adopted a decay constant  $k_V = 5.9 \text{ cm}^2 \text{ mJ}^{-1}$  which was determined for Far-UVC inactivation of aerosolized HCoV-OC43 (3) and we have used this value for simulations of both Far-UVC and upper-room devices. It is well known that different viruses and bacteria exhibit a range of susceptibility to GUV light from low-pressure mercury lamps operating primarily at 254 nm and also more complex inactivation rates including “two-stage” and “shoulder” response curves (2). In addition to the single-stage  $k_V$  value that we have adopted

for HCoV-OC43, recent studies of virus inactivation by Far-UVC light report values of  $k_V = 4.1 \text{ cm}^2 \text{ mJ}^{-1}$  for HCoV-229E (3) and  $k_V = 1.8 \text{ cm}^2 \text{ mJ}^{-1}$  for influenza H1N1 PR8 (2). Clearly, a range of susceptibility is to be expected, especially as more experimental data become available from Far-UVC inactivation experiments.

In Fig. 9, we compare our simulations for inactivation of HCoV-OC43 with eighteen commercial Far-UVC devices operating continually at the current TLV with the same simulations but for  $k_V = 3.0 \text{ cm}^2 \text{ mJ}^{-1}$  and  $k_V = 9.0 \text{ cm}^2 \text{ mJ}^{-1}$  representing both lower and higher GUV susceptibility. The different GUV susceptibilities result in the expected behavior in Fig. 9 with the larger  $k_V$  values giving more rapid inactivation for the one-time release and a lower viral load for the continual release simulations. Further study of the effects of different inactivation rates and multi-stage processes will be undertaken as more data become available for inactivation of aerosolized viruses by both Far-UVC and upper-room devices.

## DISCUSSION

In our simulations, it is clear that there is a large benefit from improved ventilation (one-time release: 37% of initial viral load for 1.4 ACH vs 2% at 6.8 ACH). It is therefore very important in this virtual classroom that the windows remain open. However, winter temperatures in St Andrews, where the modeled classroom is based, typically range from  $1^\circ\text{C}$  ( $34^\circ\text{F}$ ) to  $7^\circ\text{C}$  ( $45^\circ\text{F}$ ). It may be reasonably expected that a pupil or teacher would close the windows during these low-temperature periods. Our simulations show that, at current exposure limits, a single upper-room GUV device or 18 commercial Far-UVC devices

would reduce viral load in such a poorly ventilated room (1.4 ACH) to levels close to that of a well-ventilated room (6.8 ACH). There is therefore utility installing GUV in this virtual classroom as it provides additional protection to ventilation, including at higher ACH, and GUV would not be affected by human behavior (such as closing windows).

For this simulated classroom, and with current commercial conditions, upper-room GUV may be the system of choice as only a single unit would be required. This is because currently available commercial Far-UVC devices have narrow illumination patterns meaning that large numbers are required to match the performance of an upper-room device. As our simulations demonstrate, it is important to ensure that the entire space is irradiated with Far-UVC for optimal inactivation (Fig. 8).

Far-UVC devices are at an early stage in their development, and there is much scope for technological improvement. For example, our simulations demonstrate that they could be improved by changing to an isotropic illumination pattern so that the room coverage would be increased, thereby reducing the number of required Far-UVC devices.

Another feature of current Far-UVC devices is that some have recommended modes of operation with long off times. There are several reasons for this including high power bulbs which requires the lights to be on for short bursts in order to stay within the time-averaged UVC safety limits; including off time to prevent over-heating of the device due to the high output power of the bulbs; and minimizing the on-time so as to extend the product lifetime due to the relatively short KrCl\* bulb life, typically less than 4000 h. With a recent study indicating indoor person-to-person transmission of SARS-CoV-2 occurred in less than a minute (25), in order to provide a safe environment and

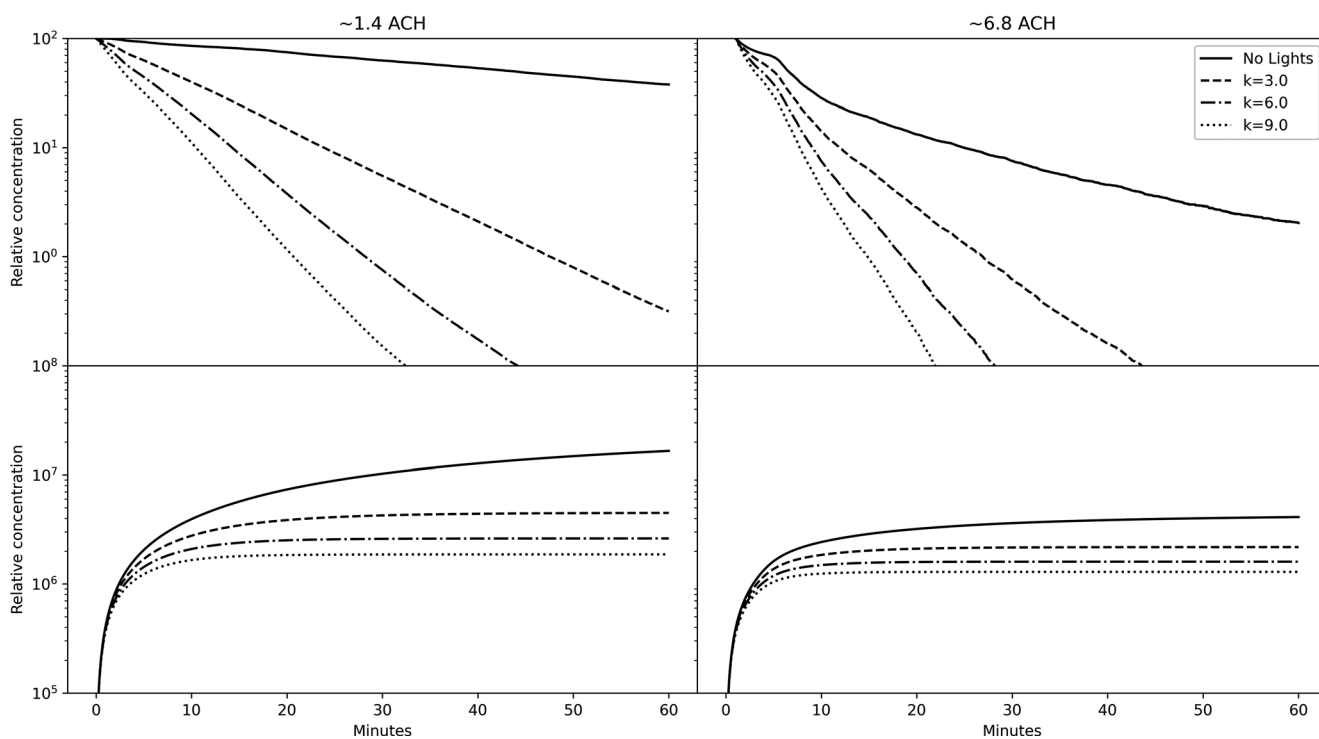


**Figure 9.** Inactivation simulations for different  $k_V$  values representing viruses that are more or less susceptible to UVC. Upper panels for one-time release of particles and lower panels for continuous release

continual air disinfection Far-UVC lights should operate with short off times (Fig. 7) or remain on continuously while rooms are occupied. This may require either the existing technology to be redesigned or for new technologies to be developed, perhaps incorporating more efficient LEDs or solid-state devices operating at Far-UVC wavelengths.

In our simulations, we have made a very conservative assumption that the 8 h exposure limit is achieved by a 2-m tall individual standing directly beneath a Far-UVC device. This is an unlikely scenario. Previous literature has shown UVC exposure from upper-room devices to be much less than anticipated due to movement within the area (26). Therefore, more accurate determination of an individual's dose when in the irradiated area could allow for a higher lamp output. Another technological improvement could be the introduction of distance sensors to change the lamp emission depending on human proximity. For example, a sensor detecting human presence at 2 m from the lamp instead of 1 m would be able to increase its output by a factor of four (making the assumption the lamp is a point source). These technological innovations would have an equivalent effect to increasing the TLV but without the need for changing legislation.

Emerging evidence is indicating that the hazard to skin and eyes from wavelengths below 230 nm is much lower than currently indicated in guidelines and legislation (7–10). As our simulations indicate, increases to the exposure limits would result in more dramatic reductions in viral load and far-UVC devices would significantly outperform upper-room UVGI and ventilation. This is tempered by the knowledge that the virus these simulations are modeled upon appears to be particularly susceptible to UVC. For other viruses and bacteria, the relationship between UVC and ventilation will be altered and such a scenario can be easily incorporated into the simulations, as demonstrated in Fig. 9.

## SUMMARY

Our simulations indicate that ventilation combined with UVGI (either upper-room UVGI or Far-UVC) can significantly reduce the viral load in a room. There are some technological limitations of current Far-UVC devices and interpretation of TLVs which are hampering Far-UVC from reaching its true potential. However, anticipated improvements in technology, reduction in costs and possible increases to exposure limits could result in Far-UVC devices providing a very important role in air disinfection.

**Acknowledgements**—The authors would like to thank Aaron Longbottom and Andrew Parker of Fluid Gravity Engineering for useful discussions about CFD and particle dissemination modeling. We acknowledge financial support from the University of St Andrews Restarting Research Funding Scheme (SARRF) which is funded through the Scottish Funding Council grant reference SFC/AN/08/020.

## REFERENCES

1. Reed, N. G. (2010) The history of ultraviolet germicidal irradiation for air disinfection. *Public Health Rep.* **125**, 15–27.
2. Kowalski, W. (2010) *Ultraviolet Germicidal Irradiation Handbook: UVGI for Air and Surface Disinfection*. Springer Science & Business Media.
3. Buonanno, M., D. Welch, I. Shuryak and D. J. Brenner (2020) Far-uv light (222 nm) efficiently and safely inactivates airborne human coronaviruses. *Sci. Rep.* **10**, 1–8.
4. Welch, D., M. Buonanno, V. Grilj, I. Shuryak, C. Crickmore, A. W. Bigelow, G. Randers-Pehrson, G. W. Johnson and D. J. Brenner (2018) Far-uv light: A new tool to control the spread of airborne-mediated microbial diseases. *Sci. Rep.* **8**, 1–7.
5. Buonanno, M., B. Ponnaiya, D. Welch, M. Stanislauskas, G. Randers-Pehrson, L. Smilenov, F. D. Lowy, D. M. Owens and D. J. Brenner (2017) Germicidal efficacy and mammalian skin safety of 222-nm uv light. *Radiat. Res.* **187**, 493–501.
6. Buonanno, M., M. Stanislauskas, B. Ponnaiya, A. W. Bigelow, G. Randers-Pehrson, Y. Xu, I. Shuryak, L. Smilenov, D. M. Owens and D. J. Brenner (2016) 207-nm UV light—A promising tool for safe low-cost reduction of surgical site infections. II: In-vivo safety studies. *PLoS One* **11**, e0138418.
7. Cadet, J. (2020) Harmless effects of sterilizing 222-nm far-uv radiation on mouse skin and eye tissues. *Photochem. Photobiol.* **96**, 949–950.
8. Fukui, T., T. Niikura, T. Oda, Y. Kumabe, H. Ohashi, M. Sasaki, T. Igarashi, M. Kunisada, N. Yamano, K. Oe, T. Matsumoto, T. Matsushita, S. Hayashi, C. Nishigori and R. Kuroda *et al.* (2020) Exploratory clinical trial on the safety and bactericidal effect of 222-nm ultraviolet c irradiation in healthy humans. *PLoS One* **15**, e0235948.
9. Kaidzu, S., K. Sugihara, M. Sasaki, A. Nishiaki, T. Igarashi and M. Tanito (2019) Evaluation of acute corneal damage induced by 222-nm and 254-nm ultraviolet light in sprague-dawley rats. *Free Radical Res.* **53**, 611–617.
10. Yamano, N., M. Kunisada, S. Kaidzu, K. Sugihara, A. Nishiaki-Sawada, H. Ohashi, A. Yoshioka, T. Igarashi, A. Ohira, M. Tanito and C. Nishigori (2020) Long-term effects of 222-nm ultraviolet radiation c sterilizing lamps on mice susceptible to ultraviolet radiation. *Photochem. Photobiol.* **96**, 853–862.
11. Barnard, I. R. M., E. Eadie and K. Wood (2020) Further evidence that far-uv for disinfection is unlikely to cause erythema or pre-mutagenic dna lesions in skin. *Photodermatol. Photoimmunol. Photomed.* **36**, 476–477.
12. Buonanno, M., D. Welch and D. J. Brenner (2021) Exposure of human skin models to krc1 excimer lamps: The impact of optical filtering. *Photochem. Photobiol.* **97**, 517–523.
13. Kitagawa, H., Y. Kaiki, K. Tadera, T. Nomura, K. Otori, N. Shigemoto, S. Takahasahi and H. Ohge (2021) Pilot study on the decontamination efficacy of an installed 222-nm ultraviolet disinfection device (care222™), with a motion sensor, in a shared bathroom. *Photodiagn. Photodyn. Ther.* **102334**.
14. Gilkeson, C. A. and C. Noakes (2013) Application of cfd simulation to predicting upper-room uvgi effectiveness. *Photochem. Photobiol.* **89**, 799–810.
15. King, M. F., C. Noakes, P. Sleight and M. Camargo-Valero (2013) Bioaerosol deposition in single and two-bed hospital rooms: A numerical and experimental study. *Buill. Environ.* **59**, 436–447.
16. Beggs, C. B. and E. J. Avital (2020). Upper-room ultraviolet air disinfection might help to reduce covid-19 transmission in buildings. *medRxiv*.
17. Buchan, A. G., L. Yang and K. D. Atkinson (2020) Predicting airborne coronavirus inactivation by far-uv in populated rooms using a high-fidelity coupled radiation-cfd model. *Sci. Rep.* **10**, 1–7.
18. Non-Ionizing Radiation Protection, I.C. (2004) Guidelines on limits of exposure to ultraviolet radiation of wavelengths between 180 nm and 400 nm (incoherent optical radiation). *Health Phys.* **87**, 171–186.
19. Governmental Industrial Hygienists, A.C. (2021). TLVs and BEIs: Threshold limit values for chemical substances and physical agents and biological exposure indices.
20. OpenFOAM. <https://openfoam.org>
21. Wood, K. and R. Reynolds (1999) A model for the scattered light contribution and polarization of the diffuse hot galactic background. *Astrophys J.* **525**, 799.
22. Barnard, I. R. M., P. Tierney, C. L. Campbell, L. McMillan, H. Moseley, E. Eadie, C. T. A. Brown and K. Wood (2018) Quantifying direct dna damage in the basal layer of skin exposed to uv radiation from sunbeds. *Photochem. Photobiol.* **94**, 1017–1025.

23. Wengraitis, S. and N. G. Reed (2012) Ultraviolet spectral reflectance of ceiling tiles, and implications for the safe use of upper-room ultraviolet germicidal irradiation. *Photochem. Photobiol.* **88**, 1480–1488.
24. Lu, J., J. Gu, K. Li, C. Xu, W. Su, Z. Lai, D. Zhou, C. Yu, B. Xu and Z. Yang (2020) Covid-19 outbreak associated with air conditioning in restaurant, guangzhou, china, 2020. *Emerg. Infect. Dis.* **26**, 1628.
25. Eichler, N., C. Thornley, T. Swadi, T. Devine, C. McElnay, J. Sherwood, C. Brunton, F. Williamson, J. Freeman, S. Berger, X. Ren, M. Storey, J. de Ligt and J. L. Geoghegan (2021) Transmission of severe acute respiratory syndrome coronavirus 2 during border quarantine and Air Travel, New Zealand (Aotearoa). *Emerg. Infect. Dis.* **27**(5), 1274–1278.
26. First, M. W., R. A. Weker, S. Yasui and E. A. Nardell (2005) Monitoring human exposures to upper-room germicidal ultraviolet irradiation. *J. Occupat Environ. Hyg.* **2**, 285–292.